

Implosion hydrodynamics of fast ignition targets

R.B. Stephens,¹ S.P. Hatchett,² M. Tabak,² C. Stoeckl,³ H. Shiraga,³ S. Fujioka,³ M. Bonino,³

A. Nikroo,¹ R. Petrasso,⁴ T.C. Sangster,³ J. Smith,¹ and K.A. Tanaka⁵

¹General Atomics, San Diego CA 92186-5608

²Lawrence Livermore National Laboratory, Livermore CA

³Laboratory for Laser Energetics, University of Rochester, Rochester NY

⁴Massachusetts Institute of Technology, Cambridge MA

⁵Institute for Laser Engineering, Osaka University, Osaka, JAPAN

ABSTRACT

The fast ignition (FI) concept requires the generation of a compact, dense, pure fuel mass accessible to an external ignition source. The current baseline FI target is a shell fitted with a reentrant cone extending to near its center. Conventional direct or indirect drive collapses the shell near the tip of the cone and then an ultra-intense laser pulse focused to the inside cone tip generates high-energy electrons to ignite the dense fuel. A theoretical and experimental investigation was undertaken of the collapse of such targets, validating modeling and exploring the tradeoffs available, in such an asymmetric geometry, to optimize compaction of the fuel and maintain the integrity of the cone. The collapse is complex. Away from the cone, the shell collapses much as does a conventional implosion, generating a hot, low-density inner core. But because of the open side hot plasma exhausts out toward the tip of the cone. This hot plasma is advantageous for implosion diagnostics; it can provide protons for angular dependent measurements of the shell wall, neutrons for temperature measurements, and self-emission for

contamination measurements. But for FI it is a liability; the hot, low-density inner core impedes the compaction of the cold fuel, lowering the implosion/burn efficiency and the gain. We discuss approaches to optimizing this shell design. Approaches to optimizing this shell design are discussed.

I. BACKGROUND

The physical outlines of Fast Ignition Fusion (FI) have been known for at least 10 years [1,2], and the basic requirements are well known [3,4]. It differs from the conventional central-hot-spot (CHS) approach in using separate drivers for the compression and ignition steps. This eliminates the need for a shock-heated low-density ignition spot surrounded by a high-density core and allows compression of the target to a uniform density $\sim 1/3$ and an ignition mass $\sim 1/10$ that required by the CHS approach; the consequent reduced energy input results in a very attractive improvement in target gain.

In the initial concept [2] the ignition pulse is provided by an ultra-high-intensity laser that bores into the lower density plasma surrounding the assembled target as far as the relativistic critical density surface. There its energy is converted into electrons that travel the rest of the distance to the dense ($\sim 300 \text{ g cm}^{-3}$) core of the target. Since the critical surface, from which these electrons would be launched, is located many hundreds of microns from the core, a variant target design containing a reentrant cone was introduced to allow electron generation closer to the core [5,6]. Small-scale integrated experiments have shown short-pulse laser heating efficiency of $\sim 25\%$ [7]. But the details of the collapse, particularly modifications caused by possible interactions between cone and shell, were unknown.

We have carried out a series of combined experiments and simulations designed to establish a detailed understanding of the compression of a reentrant cone fast ignition target. There were three major questions to address: 1) do the hydrodynamics codes, which have been exhaustively tested on spherically symmetric targets, properly capture all of the physics in these extremely

asymmetric cases, 2) do shell-cone interactions interfere with efficient assembly of a dense core, and 3) does the design space allow simultaneous core assembly and ignition access.

Initial modeling (Section II) showed that the generation of the desired uniformly dense blob of fuel was difficult; the hot central core is a robust feature. Then several combined experimental/modeling campaigns (Section III) showed reasonable efficiency in assembling a core but also a number of shell-cone interactions that must be accounted for during optimization. We discuss the various interactions in Section IV. Using this information, we then describe requirements regarding FI target optimization (Section V). We conclude (Section VI) that though the simulations are qualitatively accurate, mixing—which is omitted—is an important process shaping the collapse properties, and that there are substantial cone-shell interactions that considerably complicate the problem of developing an optimized target. Our modeling has, however, established promising directions as the foundation of a concerted design effort.

II. INITIAL MODELING

The first simulation (Fig. 1), used a typical CHS shell and drive with a cone added (the hyperboloidal tip offset from the shell center by ~ 40 mm) and with minimal central gas ($r_{\text{gas}} = 5 \times 10^{-5} \text{ g cm}^{-3}$). This target collapses to a hollow shell around a low-density core. The gas is generated by the shock from the laser drive and then, because the shell collapses faster than it can escape, is heated to ~ 400 eV by compression. Although the maximum areal density of this target ($\rho R \sim 2.2 \text{ g cm}^{-2}$) is satisfactory, the extended form this target takes at stagnation is undesirable. Unlike a CHS target, a FI target does not burn from the center out starting at the low-density core. Rather ignition occurs in the dense shell, and the resulting nuclear burn, limited to dense fuel, must travel along the thin shell. Improved collapses can be formed by

generating a larger collapse velocity from the side away from the cone than at the sides, using either an ablator, fuel, or drive asymmetry (Fig. 2). A symmetric target (as in Fig. 1) with a 10% drive asymmetry produces a much more satisfactory shape with the same ρR [Fig. 2(c)]. The collapse geometry changes rather strongly with scale size (Fig. 3); considerable work will be required to optimize this type of target.

We roughly estimated the electron beam energy required for adequate burn-up fraction. The electron beam was modeled as a monoenergetic *ion* beam ($A=1/1822$, $Z=1$) injected from a disc inside the gold cone with some initial divergence. This model should get the dE/ds of the particles about right, and includes the energy loss through the gold cone, but it neglects scattering and all self-consistent-field effects on the transport. The collimation or divergence used for injection is intended to include such effects. An electron energy of about 1.6 ± 0.1 MeV was found to minimize the total beam energy required for this capsule. Injection of such *ad hoc* electron beams suggest this mass has a reasonable chance of being ignited, yielding >20 MJ after ignition with between 30 and 150 kJ of 1 MeV electrons, for electron beam divergence of 0° and 50° respectively (Fig. 4). Capsules tuned for lower drive temperature or energy produced ρR s less than 2 g cm^{-2} . Although these could be “ignited”, they produced much lower burn-up fractions than might have been expected. In conventional hot-spot ignited capsules the fuel burn-up fraction t may be estimated as [8].

$$\phi \approx \frac{\langle \rho R \rangle}{\langle \rho R \rangle + 6 \text{ g cm}^{-2}} \quad (1)$$

where $\langle \rho R \rangle$ is the full, hot-spot plus main fuel, column density. This formula derives from the competition between fuel burning at a temperature that saturates near 40 keV, and an inrushing rarefaction that disassembles the fuel and stops the burning, and was determined for a hollow

shell geometry. We found that the burn-up fractions for implosions producing blob $\langle\rho R\rangle$'s less than $\sim 2 \text{ g cm}^{-2}$ fell off much faster than naive application of the above formula would suggest. Presumably this is because confinement in spherical or effectively spherical geometry simply lasts longer, but a fuller understanding of the confinement process in the 3-D geometry of FI is certainly warranted.

III. EXPERIMENTAL TESTS

The cryo-ignition target in Fig. 1 was then re-sized to Omega [9] drive energy, first for x-ray drive [10] and then for direct laser drive [11], to test the model predictions. X-ray drive targets [Fig. 5(a)] were driven exactly as a 1/2 mm diameter CHS shell in a scale 1 hohlraum using 14 kJ of drive power. The reentrant cone (dimensions as in the model: Opening angle 70° , the tip 40 μm from the center of the shell) was notched outside the shell to prevent an excessive x-ray flux on the cone near the shell. The direct drive targets had a $\sim 1 \text{ mm}$ diameter shell [Fig. 5(b)]. The cone base blocked one set of beams entirely. The shell was driven with 11 kJ from 15 half power and 20 full power beams. In the cases illustrated here the targets were backlit with He-like Fe- K_α radiation (6.7 keV) from a film hit with delayed beams (8 beams delayed 1.4 ns on the outside of a 7 mm foil for x-ray drive and 15 beams, delayed 1.8 ns on both sides of a 10 μm foil for direct). The sensitivity of the framing camera was determined by reference to a calibrated time integrating x-ray spectrometer [12]. The emitted spectrum, convoluted with the camera filter transmission and the spectral sensitivity of the camera [13], was compared to the backlighter intensity integrated over backlighter area (a vertical and horizontal super-Gaussian fit was used to account for the part of the backlighter hidden behind the target) and summed over

the camera frames. An identical framing on the other side of the chamber observed the self-emission (s-e) of the target without any backlighter.

The tests were made with nominally symmetric targets and symmetric drives, so we expected a collapsed geometry as in Fig. 1. A collapsed x-ray drive target is shown in Fig. 6 and direct drive targets in Fig. 7. Targets were either empty or filled with 5–10 atm of D₂ or D³He. In all cases the cone [with an initially sharp, hyperboloidal tip Fig. 6(b)] appears distorted. For the x-ray drive case (Fig. 6) there appears to be no separation between the shell and the cone. For direct drive (Fig. 7) there is a clear separation, but since the interstitial area is brighter than the backlighter, that intensity must include some s-e, which could be masking absorption from vapor. Gas-filled targets showed obvious self-emission near stagnation. Detailed investigation of these images revealed a number of shell-cone interactions occurring in fast ignition targets that must be taken into account in their design.

IV. CONE-SHELL INTERACTIONS

A. Cone Heating/Au Contamination

The fuzziness of the cone outlines in the back-lit images (especially in x-ray drive, Fig. 6) is caused by a surrounding cloud of Au vapor. An unintentional high-photon-energy component of the drive spectrum is boiling away the Au surface. The origin of the x-rays, in the x-ray drive case, comes from the non-thermal Au-M lines in the emission from the Au hohlraum (~6% of the total incident energy for our targets [14]), and from thermal emission of the laser heated CH shell in the direct drive case. In a CHS target these weakly absorbed spectral components cause a mild preheating of the imploding shell. In a reentrant cone FI target, such penetrating radiation (~1.5–4.5 keV with peak at 2–2.5 keV) is absorbed by the surface of the cone. LASNEX [15]

calculations suggest that the energy incident on the cone is $\sim 40 \text{ kJ cm}^{-2}$ in the x-ray drive case and $\sim 9 \text{ kJ cm}^{-2}$ for direct drive. In neither case is that flux easily eliminated. For x-ray drive, all of the possible hohlraum materials used for hohlraum materials emit non-thermal lines in the same energy band. For direct drive the bremsstrahlung induced by the laser-generated-hot-electrons scales with Z^2 of the shell material; it would be reduced somewhat with a Be:Cu_x shell and considerably more using a cryo-foam target (that reduces the C density by nearly an order of magnitude).

This incident energy, absorbed in $<1 \mu\text{m}$ of the Au, generates a dense vapor layer ($\sim 0.5 \text{ g cm}^{-3}$ – clearly seen in the first images of Fig. 8) that is Rayleigh-Taylor (R-T) unstable against the pressures exerted by the lower density gas escaping the collapsing shell, so mixes with it. In the x-ray drive case a filament of Au vapor can be seen to escape into the low-density core [Fig. 6(b)]. The apparent contamination is much more limited in our direct-drive experiments. The extent of that contamination cannot be measured with opacity, as in indirect drive, because of s-e from the hot core. This s-e is as bright as the backlighter in some cases and gives the illusion of a complete separation between cone and collapsed shell [as in Fig. 7(a)] unless a whole sequence is examined (Fig. 8).

Within the collapsing shell, LASNEX simulations qualitatively replicate the time evolution and shape of the s-e as well as the evolving shape of the target, but overestimate the absolute value of both s-e and opacity. The maximum s-e intensity varies at least a factor of 2 from shot to shot. Since the framing camera only detects $h\nu > 2 \text{ keV} \gg kT$, the measured intensity is extremely sensitive to the gas temperature; a reasonable assumption is that mixing, varying with laser drive, target surface and axial symmetry deviations, is the cause of both the low s-e intensity and the variability [Fig. 7(b,c)].

Near the cone, the simulations are not so accurate. They predict a sharply defined Au vapor layer that is not pushed back until near the stagnation time, and no s-e; we observe no boundary and rather bright s-e (Fig. 8). As noted above, the Au vapor boundary is hydrodynamically unstable against the CH gas stream, so the Au would be expected to mix and could diffuse into the core of the collapsing target. Any Au contamination increases the opacity of the gas in that vicinity (H is invisible and the C is ionized enough to lower its normal absorption by orders of magnitude in the low density exhaust gas), and thus the s-e brightness. It is possible to make an estimate of the amount of Au that could be mixing into that region using the s-e observed (from the opposite side) by a separate framing camera (Fig. 9). Lineouts of these s-e images (summed 60 μm transversely) show that the minimum intensity between the peaks located on the core and cone is about 1/3 of the core peak. The back-lit images at those times show a core brightness about equal to the backlighter. In that region, the core is nearly opaque, so this intensity is almost entirely s-e. In between the core and cone the image is still about as bright as the backlighter. The shell is expected to be partially transparent here, so this intensity is the sum of transmitted backlighter radiation and s-e. But we expect the s-e there to be about a third as bright as at the peak, so $\sim 1/3$ the backlighter emission is absorbed in that area. A column of Au vapor $\sim 0.15 \text{ g cm}^{-3}$ and 100 μm diameter could cause such absorption. But absorption from the low-density plasma surrounding the collapsing shell should be about that value (that absorption is visible in Fig. 9(c) on either side of the cone tip) so Au, if there is any in that area, must be at a much lower concentration. In any case, the Au doping of the core is much less than observed using x-ray drive.

B. Shell-Cone Asymmetry

The addition of a reentrant cone put a new requirement that the shell collapse to a predetermined point in front of the cone tip. A cone offset more than $\pm 10 \mu\text{m}$ causes turbulent mixing of the core with the wall and prevents an optimum collapse [Fig. 7(c,d)]. Such an offset can be caused by asymmetric drive, or shell, mis-placement or -orientation in the target chamber. It appears, in this case, that the cone axis was tilted $\sim 5^\circ$ from nominal. Since the beams under the cone are not used, this turned part of the shell toward lower intensity drive and shifted the center of collapse.

C. Cone Collapse

The cone seen in indirect drive experiments (the opaque region in Fig. 6) appears considerably blunted compared to its original shape. That is to be expected; the central gas (simulations show a density of $\sim 10\text{--}20 \text{ g cm}^{-3}$, heated to $\sim 400 \text{ eV}$, and moving at $\sim 10^7 \text{ cm s}^{-1}$ for an initially empty shell; the density is doubled and the velocity \sim halved for a filled shell) is flowing directly toward the tip, eventually punching it in, as seen in Fig. 2 (in simulations that collapse starts later for a filled shell). Since it is through that tip that the ignition energy is transmitted, the timing of that collapse is of vital interest. The simulated backlit images show that qualitatively through the position of the Au vapor; the boundary is not pushed down against the tip until just before stagnation. Experimentally, that layer vanishes somewhat earlier (Fig. 8 simulation image 3 and experimental image 1, respectively). This was investigated quantitatively using the shadow of a ledge partway down the cone as a stable reference point [Fig. 10(a)]. Fitting all the images in each shot to a 3-D model allowed determination of the fixed parameters in a sequence (cone axis tilt and ledge radius), and the height of each cone tip above its ledge as

a function of time [Fig. 10(b)]. The measured collapse rate agrees quite well with that predicted by simulation. Both indicate that the tip (initially $\sim 50\mu\text{m}$ thick) collapses by 20–30 μm before stagnation—about the cone tip thickness one would use in an ignition target—so the tip would be destroyed before the shell mass is assembled and the ignition pulse can be delivered.

D. Collapse Density

ρR_{max} was determined experimentally from backlighter absorption and with proton energy loss spectroscopy [10,11]. The backlit images used an Fe backlight ($h\nu\sim 6.7\text{ keV}$) and filter to discriminate against s-e. Absorption was determined using lineouts perpendicular to the cone axis and compared to a fit to the non-uniform backlighter intensity. The results were fitting to a uniformly dense solid sphere. X-ray drive targets appeared much more dense than direct-laser drive targets ($\sim 100\text{ mg cm}^{-2}$); possibly the result of mixed-in Au. D^3He filled direct drive targets could also be evaluated using proton energy loss spectroscopy. Detectors placed on a line-of-sight away from the cone gave similar density ($\sim 60\text{ mg cm}^{-2}$) as the absorption measurements ($\sim 80\text{ mg cm}^{-2}$).

Comparison of ρR_{max} obtained and modeled is a measure of the success achieving a clean compression (Table 1). For CHS shells, the standard of comparison is a 1-D calculation. On that basis these shells achieve $\geq 50\%$ of 1-D; a respectable number. A 2-D LASNEX calculation shows that in a reentrant cone target a substantial part of the core gas can escape (the cone tip “punctures” the target), allowing the shell to collapse to a more compact shape. So experimentally these FI targets should perform better than CHS shells on this measure.

5. FAST IGNITION TARGET OPTIMIZATION

A. High-Z Doping Of Core Gas

High-Z doping of the core gas might do no harm, since the low-density fuel is not burned in a FI target, and might actually do some good, by allowing the core to radiatively cool, lowering its pressure and allowing the surrounding shell to collapse to a smaller, more compact core. Allowing such doping puts a premium on minimizing the mixing between the hot core and collapsing shell of dense fuel (which is sensitive to such doping; adding ~ 0.1 at% Au doubles the required ignition energy [10]), so the specifications on the drive and shell for an FI target could be nearly as rigorous as those for a CHS target. If necessary, such doping could be suppressed by tamping the high-Z cone surface with a thin plastic or low-Z metal covering.

B. Shell-Cone Asymmetry

Simulations suggested that offsets $<\pm 10$ μm were acceptable. All targets were built to that specification, and most collapsed cores were satisfactorily aligned to their cone. Most potential sources of offset (drive imbalance and target placement) are also potential problems in standard CHS shells and well enough controlled that they are not a problem [16]. There is a new requirement for FI targets; apparently the cone axis alignment must be controlled to $\sim \pm 1^\circ$; that is not difficult to achieve. However building the target with sufficient accuracy is, and will remain a challenge; again nearly as rigorous as a CHS x-ray drive target.

C. Cone Collapse

The observed cone tip collapse ≥ 30 μm starting before stagnation is a serious problem as it is large enough to destroy the tip before the ignition pulse can be employed, strongly affecting the conditions in with the electron or proton beam is produced. It is a direct consequence of the

formation of a hot, (relatively) low-density core in the collapsing target (even in an initially empty shell). The amount and timing of the collapse depends sensitively on details of the drive. Using an asymmetric drive to compress it away from the cone stretches the dense shell into an extended shape that is not conducive to an efficient burn; compressing it toward the cone makes a more compact fuel core, but impacts the cone even more strongly [Fig. 3(b)]. A study of the cone collapse as a function of drive symmetry is necessary to establish the optimum configuration.

D. Collapse Density

During optimization ρR_{\max} cannot be the entire measure of performance for reentrant cone shells; compactness must also be considered. Unlike CHS, a FI target does not burn the low-density fuel in the center. A burn front must travel through dense fuel. The simulated collapses shown in Figs. 1, 2(b), and 2(c) all have $\rho R_{\max} \sim 2.2 \text{ g cm}^{-2}$, but the shell-shaped collapse in Fig. 1 should be less efficient than the compact one in Fig. 2(c). Unfortunately, accurately evaluating those differences will be difficult.

6. CONCLUSIONS

Reentrant cone FI target have been collapsed with around half the ρR_{\max} of a 1-D simulation. The disparity is presumably the result of mix—an important process in cone-targets—not included in the simulations. Mix of the cone material with the collapsed core is much smaller for direct laser drive targets than for x-ray drive, and is possibly inconsequential. However exhaust from that core strongly impacts the cone tip before the target is fully assembled; minimizing this effect, or designing the ignition pulse to accommodate it, will be a critical.

The requirements for optimizing such a target are rather different and perhaps not much less stringent than for CHS. Targets must be assembled with high precision. High mode asymmetries must be controlled to limit mixing of contaminated core gas with the dense fuel to be burned. Low mode asymmetries must be controlled to place the compressed fuel at the correct place $\pm 10 \mu\text{m}$ and to control the strength of gas flows impacting the cone tip. However, the design space available to FI target design is huge, and we have just begun to explore the possibilities.

ACKNOWLEDGMENTS

The authors are indebted to the target fabrication group at GA and the OMEGA staff at LLE for making these experiments possible. We are grateful to Dr. S.G. Glendinning (LLNL) for evaluating the drive beam imbalance in our experiments (there wasn't any) and to B. Yaakobi (LLE) for calibrated spectrometer measurements. This work was supported by the U.S. Department of Energy Office of Inertial Confinement Fusion under Cooperative Agreement No. DE-FC03-92SD19460, the University of Rochester and the New York State Energy Research and Development Authority and with the corporate support of General Atomics. The support of the DOE does not constitute an endorsement of the views expressed in this article.

REFERENCES

- [1] N.G. Basov, S.Y. Guskov and L.P. Feokistov, *J. Sov. Laser Res.* **13**, 396 (1992).
- [2] M. Tabak et al., *Phys. Plasmas* **1**, 1626 (1994).
- [3] S. Atzeni, *Phys. Plasmas* **6**, 3316 (1999).
- [4] M. Rosen, *Phys. Plasmas* **6**, 1690 (1999).
- [5] M. Tabak, J. H. Hammer, E. M. Campbell, *et al.*, Lawrence Livermore National Laboratory patent disclosure IL8826B, 1997, Lawrence Livermore National Laboratory, Livermore, CA.
- [6] R. Kodama, K. Mima, K. A. Tanaka, Y. Kitagawa, H. Fujita, K. Takahashi, A. Sunahara, K. Fujita, H. Habara, T. Jitsuno, Y. Sentoku, T. Matsushita, T. Miyakoshi, N. Miyanaga, T. Norimatsu, H. Setoguchi, T. Sonomoto, M. Tanpo, Y. Toyama, and T. Yamanaka, *Nature* **412**, 798 (2001).
- [7] R. Kodama, H. Shiraga, K. Shigemori, Y. Toyama, S. Fujioka, H. Azechi, H. Fujita, H. Habara, T. Hall, Y. Izawa, T. Jitsuno, Y. Kitagawa, K. M. Krushelnick, K. L. Lancaster, K. Mima, K. Nagai, M. Nakai, H. Nishimura, T. Norimatsu, P.A. Norreys, S. Sakabe, K. A. Tanaka, A. Youssef, M. Zepf, and T. Yamanaka, *Nature* **418** 933-934 (2002).
- [8] J.L. Lindl, "Inertial Confinement Fusion," 1998, Springer-Verlag, New York.
- [9] T.R. Boehly, D.L. Brown, R.S. Craxton, R.L. Keck, J.P. Knauer, J.H. Kelly, T.J. Kessler, S.A. Kumpan, S.J. Loucks, S.A. Letzring, F.J. Marshall, R.L. McCrory, S.F.B. Morse, W. Seka, J.M. Soures, and C.P. Verdon, *Opt. Commun.* **133**, 495-506 (1997).
- [10] R.B. Stephens et al., *Phys. Rev. Lett.* **91**, 185001 (2003).
- [11] C. Stoeckl, R. Stephens, J. A. Delettrez, S. Hatchett, C. K Li, R. Petrasso, F. Seguin, V. Smalyuk, W. Theobald, B. Yaakobi, and T. C. Sangster, "Fuel Assembly Experiments with

gas-filled cone-in-shell Fast-Ignitor Targets on OMEGA,” submitted to *Phys. Rev. Lett.* in 2005.

- [12] See National Technical Information Service Document No. DE83015439 1983: A. J. Burek and B. Yaakobi, Final Report to the National Bureau of Standards (unpublished). Copies may be ordered from the National Technical Information Service, Springfield VA 22161.
- [13] G. A. Burginyon, B. A. Jacoby, J. K. Wobser, R. D. Ernst, D. S. Ancheta, and K. G. Tirsell,, *SPIE* **1736**, 36 (1992).
- [14] P. Amendt, R. E. Turner, and O. L. Landen, *Phys. Rev. Lett.* **89**, 165001 (2002).
- [15] J. A. Harte, W. E. Alley, D. S. Bailey, J. L. Eddleman, and G. B. Zimmerman, *1996 ICF Annual Report*, Lawrence Livermore National Laboratory, Livermore, CA, Report No. UCRL-LR-105821-96, 150 (1997). Available online at <http://www.llnl.gov/nif/icf/icfpubs/annuals/96-Annual.pdf>
- [16] T. C. Sangster, J. A. Delettrez, R. Epstein, V. Yu. Glebov, V. N. Goncharov, D. R. Harding, J. P. Knauer, R. L. Keck, J. D. Kilkenny, S. J. Loucks, L. D. Lund, R. L. McCrory, P. W. McKenty, F. J. Marshall, D. D. Meyerhofere, S. F. B. Morse, S. P. Regan, P. B. Radha, S. Roberts, W. Seka, S. Skupsky, V. A. Smalyuk, C. Sorce, J. M. Soures, C. Stoeckl, and K. Thorn, *Phys. Plasmas* **10**, 1937 (2003).

FIGURE CAPTIONS

Fig. 1. NIF scale reentrant cone fast ignition target designed to absorb ~ 180 kJ of $T_{\text{rad,max}}=250$ eV radiation and be imploded to $\langle\rho R\rangle_{\text{DT}}\sim 2.2$ g cm $^{-2}$. Capsule inner radius is 790 μm , surrounded by 260 μm of DT ice and 122 μm of Cu doped Be ablator. The initial central gas density is 3×10^{-5} g cm $^{-3}$. The cone is 30 μm thick at the tip, increasing to ~ 120 μm at the outer capsule radius, with a full opening angle of 70° . The cone tip is offset (back) from the shell center by ~ 40 μm .

Fig. 2. Cross-section of imploded capsule density from target as in Fig. 1 but with a polar asymmetries in the collapse: a) the ablator was thinner on the side away from the cone, b) the fuel was thinner on the far side, and c) the target was uniform but the radiation intensity had a P_1 asymmetry, $\sim 10\%$ higher on the far side. The stagnated targets reached solid-angle-averaged ρR 's of ~ 1.8 , 2.2, and 2.2 g cm $^{-2}$, respectively.

Fig. 3. Target from Fig. 1 scaled up 1.6X and driven at $T_{\text{R,max}}=190$ eV, absorbing 380 kJ in 42 ns a) symmetrically and b) with 10% polar asymmetry.

Fig. 4. Electron beam ignition of the compressed fuel in Fig. 2(c) comparing results for divergent and collimated beams. The beams were launched from a 20 μm radius disc just inside the gold cone and given a spread of 50° fwhm in (a) and (c), and 0° in (b) and (d). (a) and (b) show energy deposition per mass, (c) and (d) show simulated neutron images at the end of energy deposition. The 50° fwhm beam required $E_{\text{beam}} \sim 150$ kJ for ignition yielding 24 MJ while the collimated beam required 30 kJ yielding 27 MJ. Both cases used 1.6 MeV electron beams.

Fig. 5. Realizations of reentrant cone fast ignition targets for (a) x-ray drive and (b) direct laser drive on Omega.

Fig. 6. Back-lit x-radiograph images of x-ray drive targets at stagnation with (a) linear and (b) log grey scale, and (c) simulation using linear grey scale. The experiment, unlike the simulation, shows a thread of opaque material leaking from the cone into a dense shell center. In (b) the thin colored line shows the original shape of the cone, the thick white line shows the border of the completely opaque region. All the images are to the same scale.

Fig. 7. Back-lit x-radiograph images of direct drive targets at stagnation (a) with only V filter to show self-emission, (b) with Fe filter to (largely) eliminate self-emission, (c) with same filter and off-center collapse. Each contained ~ 5 atm D_2 . Cone and core centerlines are drawn in (b) and (c) as guides to show the ~ 25 μm offset in (c). (d) Lineouts across the images in (b) and (c) showing that the offset limited the compression (FWHM increased from 80 to 120 μm), and reduced core gas self-emission (the apparent absorbed fraction increased from 0.65 to 0.75).

Fig. 8. Sequence of direct drive collapse images from (a) experimental shot #32387 and (b) simulated in LASNEX. The simulated images assumed a backlighter brightness $\sim 2.5 \times 10^9$ photons/sr/cm²/ns.

Fig. 9. (a) backlit and (b) self-emission radiographs of a cone target. The pictures were taken at about the same time (~ 2.2 ns after the drive pulse) from opposite sides. (b) has been horizontally flipped). (c) shows the relative self-emission intensity from (b) along the cone axis, averaged over ± 30 μm from the cone axis.

Fig. 10. (a) The actual tip height was calculated by fitting the shadow of the ledge to an ellipse whose orientation and size was held fixed for all images in a sequence and assumed to be centered under the tip. (b) Calculated tip height versus time for filled (triangles) and empty capsules (squares and Xs), and from LASNEX simulation of a gas filled capsule (smooth line). The LASNEX curve shows the “observed” tip collapse. The simulation shows the initial collapse starting ~ 0.2 ns earlier but being hidden from view by the region around it [as in Fig. 3(b)].

Table 1. Collapse metrics as measured experimentally for direct and indirect drive, and as predicted by LASNEX simulations for a reentrant cone shell with a 70° cone angle. According to the simulation, it fares better than a CHS shell collapsed under the same conditions; perhaps because the core can leak out, allowing collapse to a smaller size.

	Experiment		Simulation
	Cone-Shell		Sphere
ρR (mg/cm ²):	100/60–80	130/200	130/150
	(Uncertainty >20%)		(x-ray/laser drive)

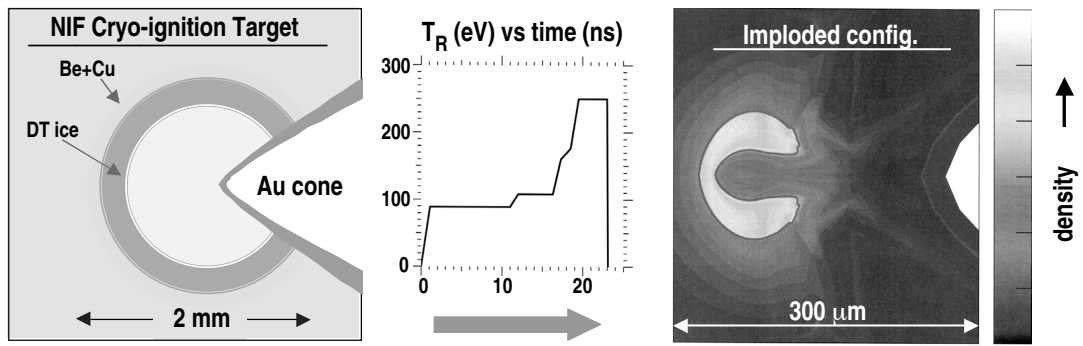


Fig. 1

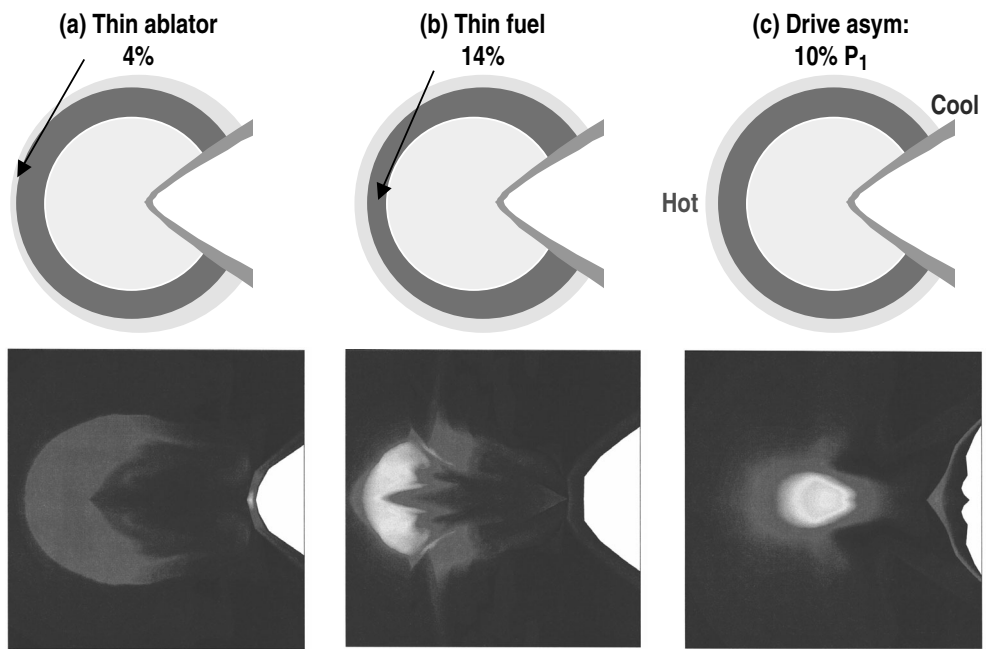


Fig. 2

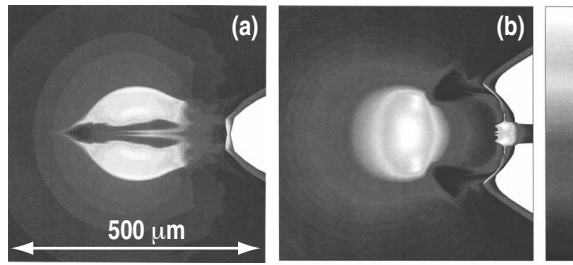


Fig. 3

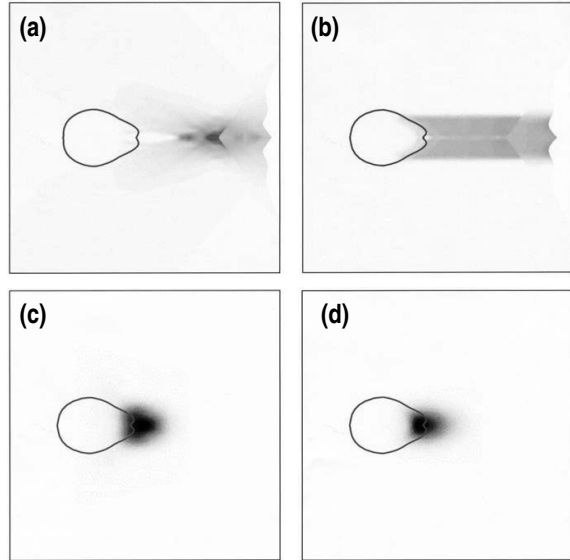


Fig. 4

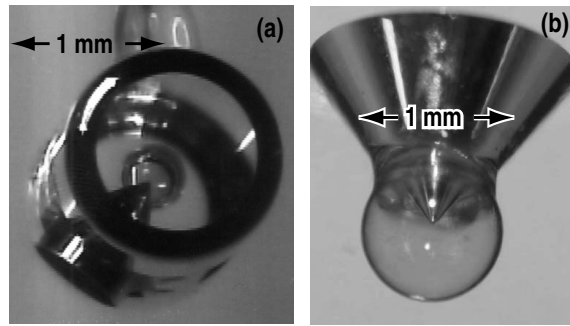


Fig. 5

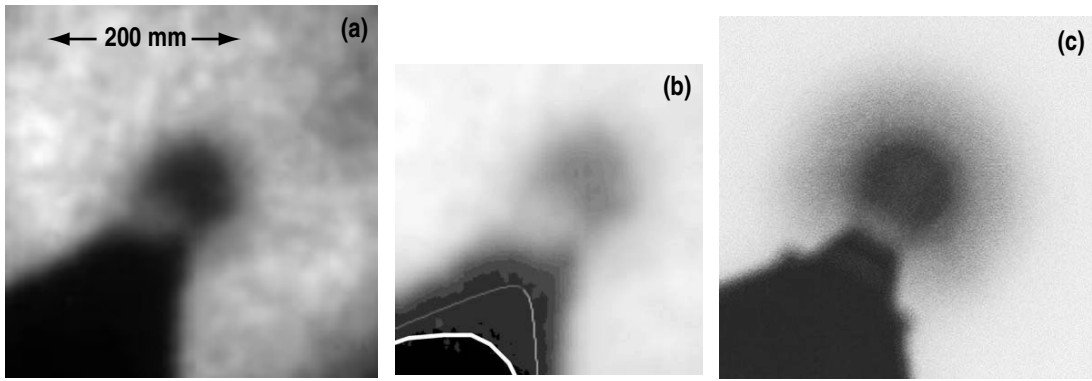


Fig. 6

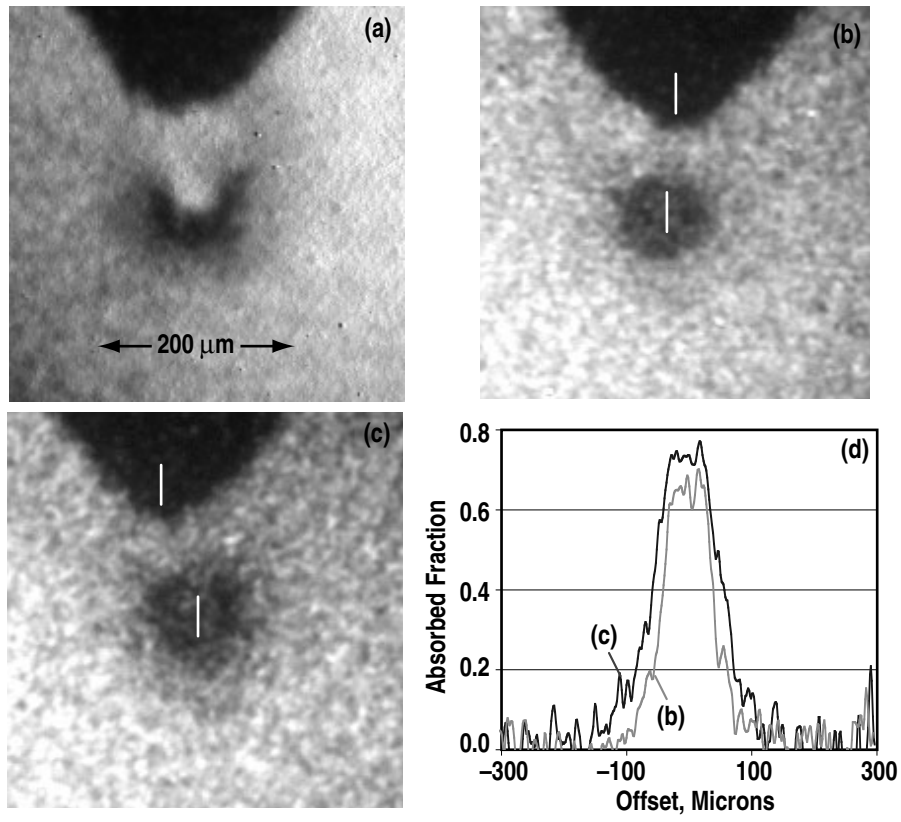


Fig. 7

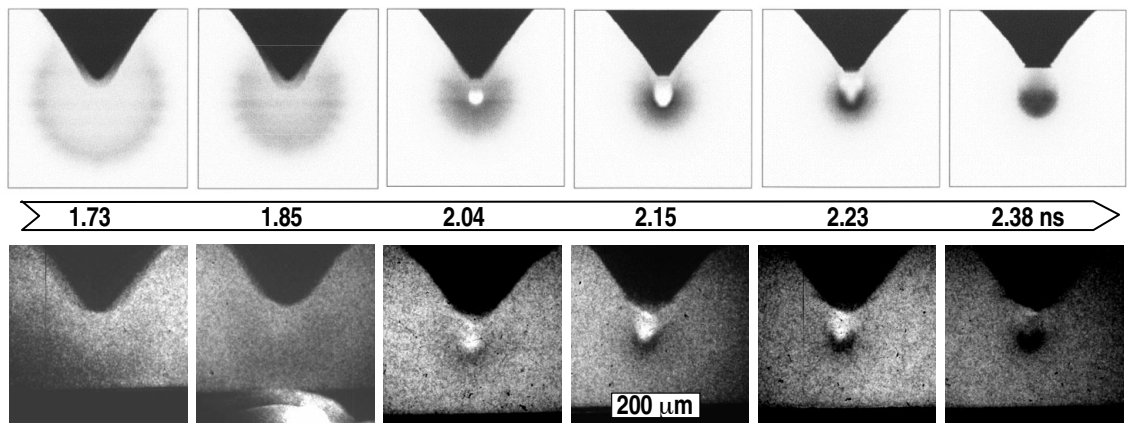


Fig. 8

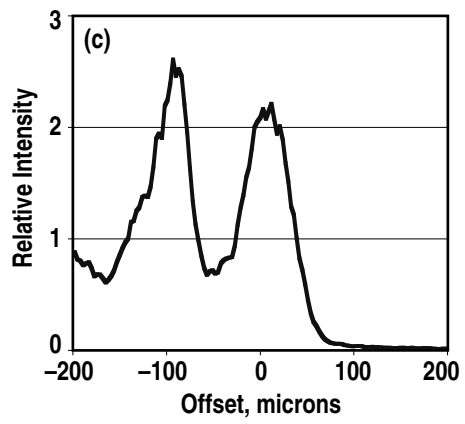
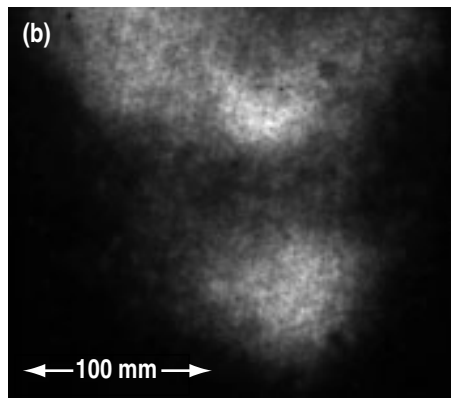
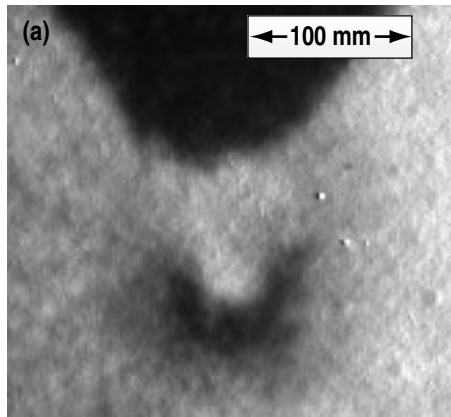


Fig. 9

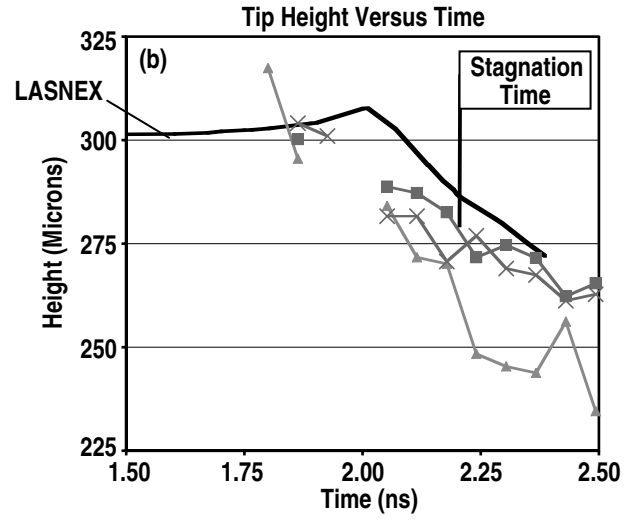
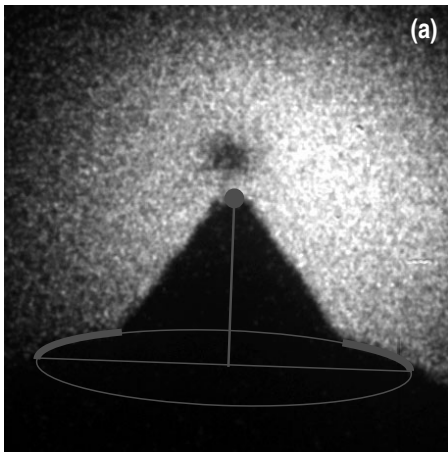


Fig. 10